Hindawi
Complexity
Volume 2019, Article ID 7931632, 15 pages
https://doi.org/10.1155/2019/7931632

Research Article

Robust Tracking Control of a Quadrotor UAV Based on Adaptive Sliding Mode Controller

Tianpeng Huang, Deqing Huang, Zhikai Wang, and Awais Shah

School of Electrical Engineering, Southwest Jiaotong University, Chengdu, China

Correspondence should be addressed to Deqing Huang; elehd@home.swjtu.edu.cn

Received 11 September 2019; Revised 12 November 2019; Accepted 26 November 2019; Published 14 December 2019

Academic Editor: Qingling Wang

In this paper, a robust adaptive sliding mode control scheme is developed for attitude and altitude tracking of a quadrotor unmanned aerial vehicle (UAV) system under the simultaneous effect of parametric uncertainties and consistent external disturbance. The underactuated dynamic model of the quadrotor UAV is first built via the Newton–Euler formalism. Considering the nonlinear and strongly coupled characteristics of the quadrotor, the controller is then designed using a sliding mode approach. Meanwhile, additional adaptive laws are proposed to further improve the robustness of the proposed control scheme against the parametric uncertainties of the system. It is proven that the control laws can eliminate the altitude and attitude tracking errors, which are guaranteed to converge to zero asymptotically, even under a strong external disturbance. Finally, numerical simulation and experimental tests are performed, respectively, to verify the effectiveness and robustness of the proposed controller, where its superiority to linear quadratic control and active disturbance rejection control has been demonstrated clearly.

1. Introduction

Quadrotor unmanned aerial vehicles (UAVs) have been the focus of robotic research in recent decades. Compared with traditional manned airplane and unmanned fixed-wing flight vehicles, quadrotor has its unique advantages, such as low cost, small size, and hovering and vertical take-off landing. As a result, quadrotor UAV is applicable in many kinds of fields, e.g., collection of photogrammetry images [1], inspection of railways [2], road detection and tracking [3], management of forest health [4], monitoring power lines [5], and package delivery [6].

To perform tasks with high reliability, the quadrotor UAV requires good flight control capabilities. Therefore, the development of a specialized controller, which is able to take into account the quadrotor's modeling nonlinearity with strongly coupled dynamics, underactuated characteristics, as well as parametric uncertainty, is always desired. Prior effort has been put towards proportional-integral-derivative (PID) control [7–9], feedback linearization [10, 11], active disturbance rejection control (ADRC) [12, 13], model predictive control [14, 15], internal model control [16], multivariable super-twisting-like-algorithm [17], back-stepping control technique [18–20], etc.

Sliding mode control (SMC) is a robust and effective method of controller design in nonlinear systems under uncertain conditions [21]. In [22], SMC is designed for a class of underactuated system, and as a typical example, the algorithm is verified in position and attitude stabilization control of a quadrotor UAV. Reinoso et al. [23] present the design of SMC for desired output tracking of a quadrotor. To overcome the potential chattering problem that is frequently encountered in standard SMC, in [24], second-order SMCs including the super-twisting sliding mode controller (ST-SMC), the modified ST-SMC (MST-SMC), and the non-singular terminal ST-SMC (NSTST-SMC) are designed and implemented in real time for the altitude tracking of a quadrotor aircraft. Meanwhile, Zhou et al. [25] propose a novel terminal sliding mode control (TSMC) scheme for tracking of the reference signal of a quadrotor UAV. Furthermore, a global fast dynamic TSMC technique is introduced in [26] to address finite-time tracking control of a

quadrotor system. Ríos et al. and Basci et al. [27, 28] develop a continuous SMC approach to deal with the robust output tracking control problem for a quadrotor. In addition, a fractional-order SMC scheme has been suggested to stabilize the attitude of quadrotors [29, 30].

Besides pure SMC, integration of SMC with other control approaches is also used to realize attitude control and to accomplish the task of trajectory tracking for quadrotor systems. More clearly, Yang et al. [31] consider a hybrid state-feedback control scheme that incorporates robust SMC and optimal linear quadratic regulator (LQR) in a hierarchical multiple-layer structure for a small-scale quadrotor. In [32], a robust nonlinear controller that combines SMC and backstepping technique is proposed, where the regular SMC for attitude inner loop is first developed to guarantee fast convergence of attitude angles and backstepping control is then applied to position loop until the desired attitude is obtained.

It is worth pointing out that, in the aforementioned works, parametric uncertainties and external disturbance have not been considered simultaneously under the framework of SMC. As a matter of fact, the parameters of a quadrotor, e.g., the moments of inertia, are difficult to be measured directly. It is also hard to get the exact values of these parameters even if they can be measured in certain ways. Meanwhile, quadrotor UAVs are inevitably subject to external disturbances during flight, such as wind gusts.

To address the problems of parameter perturbation and external disturbances, an integral predictive/nonlinear H_∞ controller with robust performance is presented in the case of aerodynamic disturbance as well as uncertain mass and inertial terms [33]. In [34], to compensate for the time-varying parameter uncertainties and external disturbances, a robust guaranteed cost controller and an optimal robust guaranteed cost controller are presented for the set-point tracking of the quadrotor UAV, respectively. A robust attitude stabilization controller is proposed, which consists of a nominal state-feedback controller and a robust compensator, for quadrotor systems under the influences of nonlinear and coupling dynamics, including parametric uncertainties, unmodeled uncertainties, and external disturbances [35]. Besides, in [36], by combining with SMC, a robust backstepping-based approach is investigated for position and attitude tracking of a quadrotor UAV subject to external disturbances and parameter uncertainties, associated with the presence of aerodynamic forces and possible wind force. Moreover, a hierarchical control strategy based on adaptive radial basis function neural networks (RBFNNs) and double-loop integral SMC is presented in [37] for the trajectory tracking of the quadrotor UAV.

In this work, the quadrotor system is considered subject to nonlinear and coupling dynamics, parametric uncertainties, and external disturbances. A novel robust adaptive sliding mode controller (ASMC) is developed to asymptotically reduce the altitude and attitude tracking errors. The main contributions of the paper are summarized as follows: (1) associated with SMC, adaptive laws are designed for simultaneous estimation of all parameters of UAV including mass, arm length, moments of inertia, and coefficients of the quadrotor system. Different from the most parameter-estimation-based controllers that always assume the availability of partial parameters of the UAV and estimate the remaining, the proposed controller shows stronger applicability for different types of quadrotor UAV. (2) The robustness of the proposed controller is guaranteed by the novel learning mechanism that takes a parallel structure. (3) The tracking convergence of the ASMC is verified by rigorous Lyapunov-based analysis, simulations, as well as real experiments.

The remainder of this paper is organized as follows. In Section 2, the dynamics of the quadrotor is presented. The control strategy is exposed in detail in Section 3. In Section 4, both simulation and experiment are conducted to verify the effectiveness of the proposed controller. Section 5 concludes the work.

2. Mathematical Model of Quadrotor UAV

In this section, the mathematical model and control principle of the quadrotor UAV are introduced. The schematic diagram of the quadrotor is shown in Figure 1, where E and B represent the earth and body frames, respectively. In flight experiment of the quadrotor UAV, rotors 1 and 4 are controlled to rotate clockwise, while rotors 2 and 3 are controlled to rotate counterclockwise. It is worth noticing that the left or right motion of the quadrotor UAV will create a roll angle by increasing (decreasing) the speeds of rotors 1 and 3 and decreasing (increasing) the speeds of rotors 2 and 4. Meanwhile, in order to obtain the pitch angle around the y-axis, the quadrotor can be controlled by increasing (decreasing) the speeds of rotors 1 and 2 and decreasing (increasing) the speeds of rotors 3 and 4. Furthermore, to rotate the quadrotor around the z-axis, it is suggested to increase (decrease) the speeds of rotors 1 and 4 and decrease (increase) the speeds of rotors 2 and 3. In addition, taking-off/landing tasks can be accomplished by increasing or decreasing all the rotors' speed uniformly.

As usual, the following assumptions are given to make the consequent controller design and analysis rigorous [10, 38]:

(i) The structure of the quadrotor UAV is rigid, and there are no internal forces or deformations

(ii) The structure of the quadrotor UAV is symmetrical

(iii) The center of mass and the origin of body frame coincide

(iv) The earth frame is an inertial frame

The six degrees of freedom of the quadrotor UAV are defined as

$$[x, y, z, \phi, \theta, \varphi] \in \mathbf{R}^6, \tag{1}$$

where $[x, y, z]$ is the position vector relative to the inertial frame E and $[\phi, \theta, \varphi]$ denotes the vector of the roll angle around the x-axis, the pitch angle around the y-axis, as well as the yaw angle around the z-axis. The rotation matrices around each of the three axes are

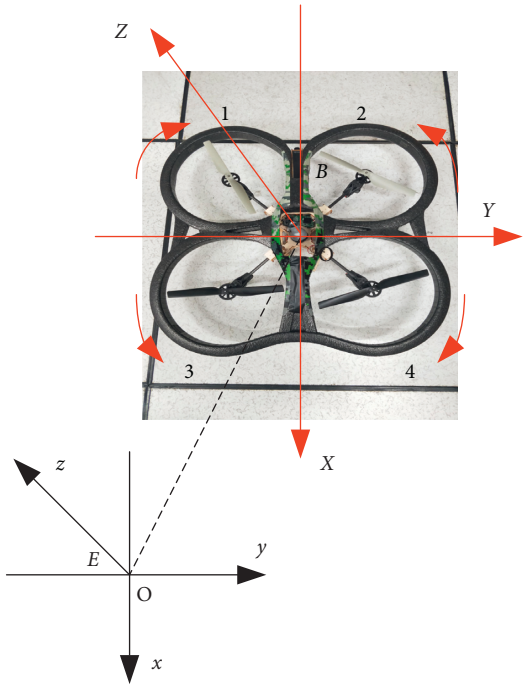

Figure 1: Diagram of quadrotor UAV.

$$R_\phi = \begin{bmatrix} 1 & 0 & 0 \\ 0 & \cos\phi & \sin\phi \\ 0 & -\sin\phi & \cos\phi \end{bmatrix}, \tag{2}$$

$$R_\theta = \begin{bmatrix} \cos\theta & 0 & -\sin\theta \\ 0 & 1 & 0 \\ \sin\theta & 0 & \cos\theta \end{bmatrix}, \tag{3}$$

$$R_\varphi = \begin{bmatrix} \cos\varphi & \sin\varphi & 0 \\ -\sin\varphi & \cos\varphi & 0 \\ 0 & 0 & 1 \end{bmatrix}. \tag{4}$$

As such, the rotation matrix from the body frame to the earth frame can be expressed as

$$R_{\mathrm{BE}} = \left(R_\phi R_\theta R_\varphi\right)^T, \tag{5}$$

where $(\cdot)^T$ denotes the transpose of matrix $(\cdot)$.

In the following, the translational and rotational dynamics of the quadrotor UAV will be exploited consequently. We first address the translational dynamics. Notice that the total lift force generated by the rotors can be given in the body frame as

$$F_T^b = [0, 0, U_1]^T, \tag{6}$$

with $U_1 \triangleq (F_1 + F_2 + F_3 + F_4)$ being the actual altitude control input, where F_i is the lift force generated by the ith rotor, $i = 1, \ldots, 4$. According to (5) and (6), the total lift force in the earth frame is then

$$F_l^e = R_{\mathrm{BE}} F_T^b. \tag{7}$$

Meanwhile, the air resistance is proportional to the flight speed of the quadrotor and can be expressed as

$$F_r^e = \left[k_x \dot{x}, k_y \dot{y}, k_z \dot{z}\right]^T, \tag{8}$$

where k_x, k_y, and k_z are the air resistance coefficients in the three directions. Moreover, the effect of gravity of the quadrotor can be described in the earth frame as

$$F_g^e = [0, 0, mg]^T, \tag{9}$$

where m is the mass of quadrotor. In summary, applying Newton's second law, the translational dynamics of the quadrotor UAV subjected to external disturbance can be obtained by (2)–(9) [14, 27].

$$\begin{aligned} \ddot{x} &= \frac{U_1(\sin\theta\cos\phi\cos\varphi + \sin\phi\sin\varphi) - k_x\dot{x}}{m} + d_x, \\ \ddot{y} &= \frac{U_1(\sin\theta\cos\phi\sin\varphi - \sin\phi\cos\varphi) - k_y\dot{y}}{m} + d_y, \\ \ddot{z} &= \frac{U_1(\cos\phi\cos\theta) - k_z\dot{z} - mg}{m} + d_z, \end{aligned} \tag{10}$$

where d_x, d_y, and d_z represent the effect of wind gusts on the translational accelerations in the form of additive external disturbances.

Then, the rotational dynamics of the quadrotor UAV are addressed. Let the vector $[p, q, r]$ represent the quadrotor's angular velocity in the body frame. The angular motion dynamics of the quadrotor can be expressed as [13, 16]

$$\begin{aligned} M_x &= J_x\dot{p} + \left(J_z - J_y\right)qr, \\ M_y &= J_y\dot{q} + \left(J_x - J_z\right)pr, \\ M_z &= J_z\dot{r} + \left(J_y - J_x\right)pq, \end{aligned} \tag{11}$$

where M_x, M_y, and M_z are the components of the resultant torque acting on the quadrotor in the three directions of x, y, and z, respectively, and J_x, J_y, and J_z are the inertias of the quadrotor around x, y, and z, respectively.

Meanwhile, let M_{lx}, M_{ly}, and M_{lz} denote the components of the lifting torque of the quadrotor in the three directions of x, y, and z, respectively. They can be expressed as [32]

$$\begin{aligned} M_{lx} &= LU_2, \\ M_{ly} &= LU_3, \\ M_{lz} &= fU_4, \end{aligned} \tag{12}$$

where L is the arm length of the quadrotor and f is the scaling factor from force to moment. In addition, U_2, U_3, and U_4 are attitude control inputs and defined as $U_2 \triangleq (F_1 + F_3 - F_2 - F_4)$, $U_3 \triangleq (F_3 + F_4 - F_1 - F_2)$, and $U_4 \triangleq (F_1 + F_4 - F_2 - F_3)$, respectively.

Besides, the quadrotor is subject to gyroscopic torque during flight, whose components M_{gx}, M_{gy}, and M_{gz} around the x, y, and z axes, respectively, are given by [32]

$$\begin{aligned} M_{gx} &= J_r q\Omega_{11}, \\ M_{gy} &= J_r p\Omega_{11}, \\ M_{gz} &= 0. \end{aligned} \tag{13}$$

In (13), J_r is the inertia of each propeller and $\Omega_{11} \triangleq \Omega_2 + \Omega_3 - \Omega_1 - \Omega_4$, where Ω_i, $i = 1, \ldots, 4$ stands for the angular speed of the ith propeller.

Considering (11)–(13), the angular motion dynamics of the quadrotor can be rewritten in the following form:

$$\begin{aligned} J_x\dot{p} &= \left(J_y - J_z\right)qr - J_r q\Omega_{11} + LU_2, \\ J_y\dot{q} &= \left(J_z - J_x\right)pr + J_r p\Omega_{11} + LU_3, \\ J_z\dot{r} &= \left(J_x - J_y\right)pq + fU_4. \end{aligned} \tag{14}$$

Compared with the brushless motor, the propeller is light. Hence, it is reasonable to ignore the moment of inertia caused by the propellers here [26]. Notice that the transformation matrix from $[\phi, \theta, \varphi]$ to $[p, q, r]$ is given by [16, 17]

$$\begin{bmatrix} \dot{\phi} \\ \dot{\theta} \\ \dot{\varphi} \end{bmatrix} = \begin{bmatrix} 1 & \sin\phi\tan\theta & \cos\phi\tan\theta \\ 0 & \cos\phi & -\sin\phi \\ 0 & \dfrac{\sin\phi}{\cos\theta} & \dfrac{\cos\phi}{\cos\theta} \end{bmatrix} \begin{bmatrix} p \\ q \\ r \end{bmatrix}. \tag{15}$$

To ensure flight safety, the attitude angles of the quadrotor are always kept small purposely during the flight. Thus, it follows from (15) that $[\dot{\phi}, \dot{\theta}, \dot{\varphi}]^T \approx [p, q, r]^T$ [39]. In consequence, the rotational dynamics of the quadrotor subjected to external disturbance [14, 27] can be derived from (14):

$$\begin{aligned} \ddot{\phi} &= \frac{\left(J_y - J_z\right)\dot{\theta}\dot{\varphi} - J_r\dot{\theta}\Omega_{11} + LU_2}{J_x} + d_\phi, \\ \ddot{\theta} &= \frac{\left(J_z - J_x\right)\dot{\phi}\dot{\varphi} + J_r\dot{\phi}\Omega_{11} + LU_3}{J_y} + d_\theta, \\ \ddot{\varphi} &= \frac{\left(J_x - J_y\right)\dot{\phi}\dot{\theta} + fU_4}{J_z} + d_\varphi, \end{aligned} \tag{16}$$

where the terms d_ϕ, d_θ, and d_φ denote the effect of wind gusts on the quadrotor's angular accelerations in the form of additive external disturbances.

3. Controller Design and Stability Analysis

In this section, a robust ASMC scheme is proposed for the quadrotor UAV system with the goal of tracking the desired altitude and attitude in the presence of parametric uncertainties and consistent external disturbance. The whole control scheme is depicted in Figure 2. It is worth mentioning that although dynamical coupling exists between the translational dynamics (10) and the rotational dynamics (16), U_i, $i = 1, \ldots, 4$ can be designed separately [26, 40].

Remark 1. In the control of the quadrotor, the changes of the states ϕ and θ will result in movement in the x and y directions, respectively. Therefore, instead of considering the full six degrees of freedom of the UAV, it is sufficient to control the four degrees of freedom (ϕ, θ, φ, and z) only. In this regard, the considered quadrotor UAV system has a fully actuated dynamic model [38], where four independent control variables are to be designed.

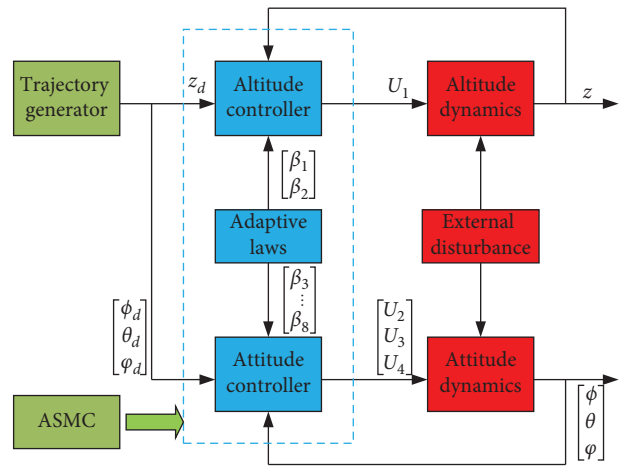

Figure 2: The proposed control scheme.

3.1. The State-Space Model of Quadrotor UAV.

Let

$$\mathbf{x} = \left[x_1, \ldots, x_{12}\right]^T, \tag{17}$$

where $x_1 = x$, $x_2 = \dot{x}$, $x_3 = y$, $x_4 = \dot{y}$, $x_5 = z$, $x_6 = \dot{z}$, $x_7 = \phi$, $x_8 = \dot{\phi}$, $x_9 = \theta$, $x_{10} = \dot{\theta}$, $x_{11} = \varphi$, and $x_{12} = \dot{\varphi}$. Then, the dynamic system of the quadrotor UAV, (10) and (16), can be reformulated in the state space:

$$\dot{x} = \begin{cases} x_2, \\ \dfrac{U_1\left(\sin x_9 \cos x_7 \cos x_{11} + \sin x_7 \sin x_{11}\right) - k_x x_2}{m} + d_x, \\ x_4, \\ \dfrac{U_1\left(\sin x_9 \cos x_7 \sin x_{11} - \sin x_7 \cos x_{11}\right) - k_y x_4}{m} + d_y, \\ x_6, \\ \dfrac{U_1 \cos x_7 \cos x_9 - k_z x_6 - mg}{m} + d_z, \\ x_8, \\ \dfrac{\left(J_y - J_z\right)x_{10}x_{12} + LU_2}{J_x} + d_\phi, \\ x_{10}, \\ \dfrac{\left(J_z - J_x\right)x_8 x_{12} + LU_3}{J_y} + d_\theta, \\ x_{12}, \\ \dfrac{\left(J_x - J_y\right)x_8 x_{10} + fU_4}{J_z} + d_\varphi, \end{cases} \tag{18}$$

where the altitude controller U_1 and the roll, pitch, and yaw controllers U_i, $i = 2, \ldots, 4$ will be designed under the framework of ASMC.

To make the subsequent analysis concise and readable, some of the involved disturbance components in (18) are rescaled as $\widetilde{d}_z \triangleq md_z$, $\widetilde{d}_\phi \triangleq (J_x/L)d_\phi$, $\widetilde{d}_\theta \triangleq (J_y/L)d_\theta$, and $\widetilde{d}_\varphi \triangleq (J_z/f)d_\varphi$, and some of the parameters are redefined as $\beta_1 \triangleq m$, $\beta_2 \triangleq k_z$, $\beta_3 \triangleq J_x/L$, $\beta_4 \triangleq (J_y - J_z)/L$, $\beta_5 \triangleq J_y/L$, $\beta_6 \triangleq (J_z - J_x)/L$, $\beta_7 \triangleq J_z/f$, and $\beta_8 \triangleq (J_x - J_y)/f$. Moreover, let $\widehat{\beta}_i$ denote the estimation of β_i, $i = 1, \ldots, 8$. Then, $\widetilde{\beta}_i \triangleq \beta_i - \widehat{\beta}_i$ is the estimation error.

Assumption 1. It is assumed that all the disturbances are uniformly bounded, i.e., $|d_x| \leq \eta_x$, $|d_y| \leq \eta_y$, $|\widetilde{d}_z| \leq \eta_1$, $|\widetilde{d}_\phi| \leq \eta_2$, $|\widetilde{d}_\theta| \leq \eta_3$, and $|\widetilde{d}_\varphi| \leq \eta_4$ with known positive constants η_x, η_y, and η_j, $j = 1, \ldots, 4$.

Assumption 2. In the design of controller for the quadrotor, to avoid any singularity, we set [32, 33, 41]

$$-\frac{\pi}{2} < x_7 < \frac{\pi}{2}, \tag{19a}$$

$$-\frac{\pi}{2} < x_9 < \frac{\pi}{2}. \tag{19b}$$

3.2. Altitude Controller Design. We first address U_1. Define the altitude error as

$$e_z = x_{5d} - x_5, \tag{20}$$

where x_{5d} is the desired altitude, and set the sliding surface as

$$s_1 = c_1 e_z + \dot{e}_z, \tag{21}$$

with c_1 being a positive constant.

The control law U_1 of altitude is designed as

$$U_1 = \frac{1}{\cos x_7 \cos x_9}\Big(\widehat{\beta}_1\left(c_1\dot{e}_z + \ddot{x}_{5d} + g\right) + \widehat{\beta}_2 x_6 + \eta_1 \operatorname{sgn}(s_1) + k_1 s_1\Big), \tag{22}$$

where $\operatorname{sgn}(\cdot)$ denotes the signum function, k_1 a positive constant, and $\widehat{\beta}_j$, $j = 1, 2$ are learned in the following way:

$$\begin{aligned} \dot{\widehat{\beta}}_1 &= \gamma_1 s_1\left(c_1\dot{e}_z + \ddot{x}_{5d} + g\right), \\ \dot{\widehat{\beta}}_2 &= \gamma_2 s_1 x_6, \end{aligned} \tag{23}$$

where γ_1 and γ_2 are positive learning gains.

The first main result of the paper is summarized as follows.

Theorem 1. *Consider the altitude dynamic model of the quadrotor UAV in the state-space form (18) with controllers (22) and adaptive laws (23). Under Assumptions 1 and 2, the altitude output tracking error of the closed-loop system is guaranteed to converge to zero asymptotically, i.e., $e_z \longrightarrow 0$ as $t \longrightarrow \infty$.*

Proof 1. Define the following Lyapunov function candidate:

$$V_z = \frac{1}{2}ms_1^2 + \frac{1}{2\gamma_1}\widetilde{\beta}_1^2 + \frac{1}{2\gamma_2}\widetilde{\beta}_2^2, \tag{24}$$

whose time derivative is

$$\dot{V}_z = ms_1\dot{s}_1 + \frac{1}{\gamma_1}\widetilde{\beta}_1\dot{\widetilde{\beta}}_1 + \frac{1}{\gamma_2}\widetilde{\beta}_2\dot{\widetilde{\beta}}_2. \tag{25}$$

For the first term on the right-hand side of (25), notice from (20) and (21) that the derivative of s_1 is given by

$$\begin{aligned} \dot{s}_1 &= c_1\dot{e}_z + \ddot{e}_z \\ &= c_1\dot{e}_z + \ddot{x}_{5d} - \dot{x}_6. \end{aligned} \tag{26}$$

By virtue of (26) and the sixth equation in (18), it follows that

$$\begin{aligned} ms_1\dot{s}_1 &= ms_1\left(c_1\dot{e}_z + \ddot{x}_{5d} - \dot{x}_6\right) \\ &= s_1\left(m\left(c_1\dot{e}_z + \ddot{x}_{5d}\right) - \left(U_1\left(\cos x_7 \cos x_9\right) - k_z x_6 - mg + \widetilde{d}_z\right)\right) \\ &= s_1 m\left(c_1\dot{e}_z + \ddot{x}_{5d}\right) + s_1 mg + s_1 k_z x_6 - s_1 U_1\left(\cos x_7 \cos x_9\right) - s_1\widetilde{d}_z \\ &= m\left(s_1\left(c_1\dot{e}_z + \ddot{x}_{5d} + g\right)\right) + k_z s_1 x_6 - s_1 U_1\left(\cos x_7 \cos x_9\right) - s_1\widetilde{d}_z. \end{aligned} \tag{27}$$

Further substituting the altitude controller (22) into (27) renders to

$$\begin{aligned} ms_1\dot{s}_1 &= \beta_1\left(s_1\left(c_1\dot{e}_z + \ddot{x}_{5d} + g\right)\right) + \beta_2\left(s_1 x_6\right) - \widehat{\beta}_1\left(s_1\left(c_1\dot{e}_z + \ddot{x}_{5d} + g\right)\right) - \widehat{\beta}_2\left(s_1 x_6\right) - s_1\eta_1\operatorname{sgn}\left(s_1\right) - k_1 s_1^2 - s_1\widetilde{d}_z \\ &= \widetilde{\beta}_1\left(s_1\left(c_1\dot{e}_z + \ddot{x}_{5d} + g\right)\right) + \widetilde{\beta}_2\left(s_1 x_6\right) - s_1\eta_1\operatorname{sgn}\left(s_1\right) - k_1 s_1^2 - s_1\widetilde{d}_z. \end{aligned} \tag{28}$$

Applying (28) into (25) yields

$$\dot{V}_z = \widetilde{\beta}_1\left(s_1\left(c_1\dot{e}_z + \ddot{x}_{5d} + g\right)\right) + \widetilde{\beta}_2\left(s_1 x_6\right) - s_1\eta_1\operatorname{sgn}\left(s_1\right) - k_1 s_1^2 - s_1\widetilde{d}_z + \frac{1}{\gamma_1}\widetilde{\beta}_1\dot{\widetilde{\beta}}_1 + \frac{1}{\gamma_2}\widetilde{\beta}_2\dot{\widetilde{\beta}}_2. \tag{29}$$

Since $\dot{\widetilde{\beta}}_1 = -\dot{\widehat{\beta}}_1$ and $\dot{\widetilde{\beta}}_2 = -\dot{\widehat{\beta}}_2$ by the definitions of $\widetilde{\beta}_1$ and $\widetilde{\beta}_2$, (29) implies that

$$\dot{V}_z = \widetilde{\beta}_1\left(s_1\left(c_1\dot{e}_z + \ddot{x}_{5d} + g\right) - \frac{1}{\gamma_1}\dot{\widehat{\beta}}_1\right) + \widetilde{\beta}_2\left(s_1 x_6 - \frac{1}{\gamma_2}\dot{\widehat{\beta}}_2\right) - s_1\eta_1\operatorname{sgn}\left(s_1\right) - k_1 s_1^2 - s_1\widetilde{d}_z. \tag{30}$$

Finally, by substituting the adaptive laws (23) into (30) and adopting the relationship $|\widetilde{d}_z| \leq \eta_1$,

$$\begin{aligned}\dot{V}_z &= -s_1\eta_1\operatorname{sgn}(s_1) - k_1 s_1^2 - s_1\tilde{d}_z \\ &= -\eta_1|s_1| - k_1 s_1^2 - s_1\tilde{d}_z \\ &\le -k_1 s_1^2 \le 0,\end{aligned} \tag{31}$$

yielding that $\dot{V}_z = 0$ if and only if $s_1 = 0$. Define the set of $\dot{V}_z = 0$ as Θ_1, that is, $\Theta_1 = \{(s_1) \mid \dot{V}_z = 0\}$. Moreover, Ξ_1 is defined as the largest invariant set in Θ_1. Obviously, the largest invariant set Ξ_1 only includes the point $s_1 = 0$. Therefore, the closed-loop system is asymptotically stabilized, i.e., $s_1 \longrightarrow 0$ when $t \longrightarrow \infty$ according to LaSalle's invariance principle [42]. Observing the detailed expression of the sliding surface (21), the asymptotical convergence of s_1 directly gives that of e_z. □

3.3. Attitude Controller Design. Now, we are in the position of the attitude controller design, i.e., the control schemes for the roll, pitch as well as yaw channels. We first address the controller of roll channel based on ASMC.

Define the tracking error of roll angle

$$e_\phi = x_{7d} - x_7, \tag{32}$$

and the corresponding sliding surface

$$s_2 = c_2 e_\phi + \dot{e}_\phi, \tag{33}$$

where x_{7d} is the desired roll angle and c_2 is a positive constant. The control law for U_2 is designed as

$$U_2 = \eta_2\operatorname{sgn}(s_2) + k_2 s_2 + \hat{\beta}_3\left(c_2\dot{e}_\phi + \ddot{x}_{7d}\right) - \hat{\beta}_4 x_{10}x_{12}, \tag{34}$$

where k_2 is a positive constant. The parametric adaptive laws for $\hat{\beta}_3$ and $\hat{\beta}_4$ are set to be

$$\begin{aligned}\dot{\hat{\beta}}_3 &= \gamma_3 s_2\left(c_2\dot{e}_\phi + \ddot{x}_{7d}\right), \\ \dot{\hat{\beta}}_4 &= -\gamma_4 s_2 x_{10}x_{12},\end{aligned} \tag{35}$$

where γ_3 and γ_4 are two positive learning gains.

The second main result of the paper is summarized as follows.

Theorem 2. *Consider the dynamic model of the quadrotor UAV in the state-space form (18) with controller (34) and adaptive laws (35). Under Assumption 1, the roll output tracking error of the closed-loop system is guaranteed to converge to zero asymptotically, i.e., $e_\phi \longrightarrow 0$ as $t \longrightarrow \infty$.*

Proof 2. Define the following candidate of Lyapunov function

$$V_\phi = \frac{1}{2}\frac{J_x}{L}s_2^2 + \frac{1}{2\gamma_3}\tilde{\beta}_3^2 + \frac{1}{2\gamma_4}\tilde{\beta}_4^2. \tag{36}$$

Differentiating V_ϕ with respect to time yields

$$\dot{V}_\phi = \frac{J_x}{L}s_2\dot{s}_2 + \frac{1}{\gamma_3}\tilde{\beta}_3\dot{\tilde{\beta}}_3 + \frac{1}{\gamma_4}\tilde{\beta}_4\dot{\tilde{\beta}}_4, \tag{37}$$

Table 1: The model parameters of the quadrotor UAV in simulation [34].

Symbol	Value	Unit
M	2.33	kg
g	9.8	m/s^2
l	0.4	m
I_x	0.16	kg m^2
I_y	0.16	kg m^2
I_z	0.32	kg m^2
k_x	0.008	N/m
k_y	0.008	N/m
k_z	0.012	N/m
f	0.05	m

Table 2: Controller parameters in the proposed ASMC.

Variable	Value
c_1	1
k_1	2500
η_1	10
β_1	40
β_2	0.005
c_2	4
k_2	20
η_2	10
β_3	2.2
β_4	100
c_3	4
k_3	20
η_3	10
β_5	2.2
β_6	100
c_4	4
k_4	1000
η_4	10
β_7	50
β_8	10

where, by (32) and (33), $\dot{s}_2$ satisfies

$$\begin{aligned}\dot{s}_2 &= c_2\dot{e}_\phi + \ddot{e}_\phi \\ &= c_2\dot{e}_\phi + \ddot{x}_{7d} - \dot{x}_8.\end{aligned} \tag{38}$$

Using the eighth equation in (18) and (38), the first term on the right-hand side of (37) can be rewritten as

$$\begin{aligned}\frac{J_x}{L}s_2\dot{s}_2 &= \frac{J_x}{L}s_2\left(c_2\dot{e}_\phi + \ddot{x}_{7d} - \dot{x}_8\right) \\ &= s_2\left(\frac{J_x}{L}\left(c_2\dot{e}_\phi + \ddot{x}_{7d}\right) - \left(U_2 + \frac{J_y - J_z}{L}x_{10}x_{12} + \tilde{d}_\phi\right)\right) \\ &= s_2\frac{J_x}{L}\left(c_2\dot{e}_\phi + \ddot{x}_{7d}\right) - s_2U_2 - s_2\frac{J_y - J_z}{L}x_{10}x_{12} - s_2\tilde{d}_\phi.\end{aligned} \tag{39}$$

By the definitions of $\tilde{\beta}_3$ and $\tilde{\beta}_4$ and substituting the roll controller (34) into (39), we have

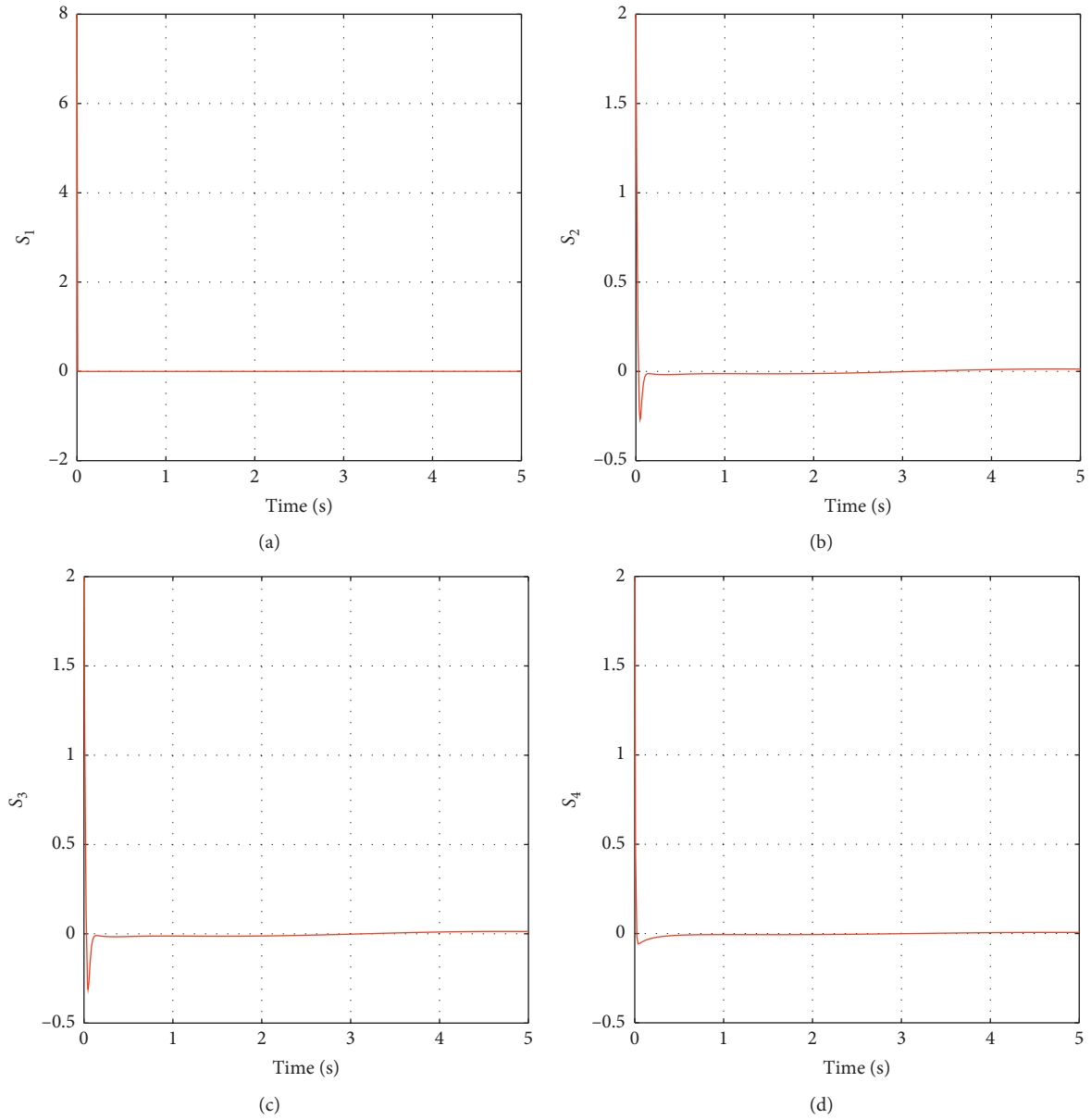

FIGURE 3: The time histories of the sliding surfaces.

$$\begin{aligned}\frac{J_x}{L}s_2\dot{s}_2 &= \beta_3 s_2\left(c_2\dot{e}_\phi + \ddot{x}_{7d}\right) - \beta_4 s_2 x_{10}x_{12} - \widehat{\beta}_3 s_2\left(c_2\dot{e}_\phi + \ddot{x}_{7d}\right)\\ &\quad + \widehat{\beta}_4 s_2 x_{10}x_{12} - s_2\eta_2\mathrm{sgn}\left(s_2\right) - k_2 s_2^2 - s_2\widetilde{d}_\phi\\ &= \widetilde{\beta}_3\left(s_2\left(c_2\dot{e}_\phi + \ddot{x}_{7d}\right)\right) - \widetilde{\beta}_4 s_2 x_{10}x_{12} - s_2\eta_2\mathrm{sgn}\left(s_2\right)\\ &\quad - k_2 s_2^2 - s_2\widetilde{d}_\phi.\end{aligned} \tag{40}$$

Then, combining (40) and (37) yields

$$\begin{aligned}\dot{V}_\phi &= \widetilde{\beta}_3\left(s_2\left(c_2\dot{e}_\phi + \ddot{x}_{7d}\right)\right) - \widetilde{\beta}_4 s_2 x_{10}x_{12} + \frac{1}{\gamma_3}\widetilde{\beta}_3\dot{\widetilde{\beta}}_3 + \frac{1}{\gamma_4}\widetilde{\beta}_4\dot{\widetilde{\beta}}_4\\ &\quad - s_2\eta_2\mathrm{sgn}\left(s_2\right) - k_2 s_2^2 - s_2\widetilde{d}_\phi.\end{aligned} \tag{41}$$

Since $\dot{\widetilde{\beta}}_3 = -\dot{\widehat{\beta}}_3$ and $\dot{\widetilde{\beta}}_4 = -\dot{\widehat{\beta}}_4$, it follows from (41) that

$$\begin{aligned}\dot{V}_\phi &= \widetilde{\beta}_3\left(s_2\left(c_2\dot{e}_\phi + \ddot{x}_{7d}\right) - \frac{1}{\gamma_3}\dot{\widehat{\beta}}_3\right) - \widetilde{\beta}_4\left(s_2 x_{10}x_{12} + \frac{1}{\gamma_4}\dot{\widehat{\beta}}_4\right)\\ &\quad - s_2\eta_2\mathrm{sgn}\left(s_2\right) - k_2 s_2^2 - s_2\widetilde{d}_\phi.\end{aligned} \tag{42}$$

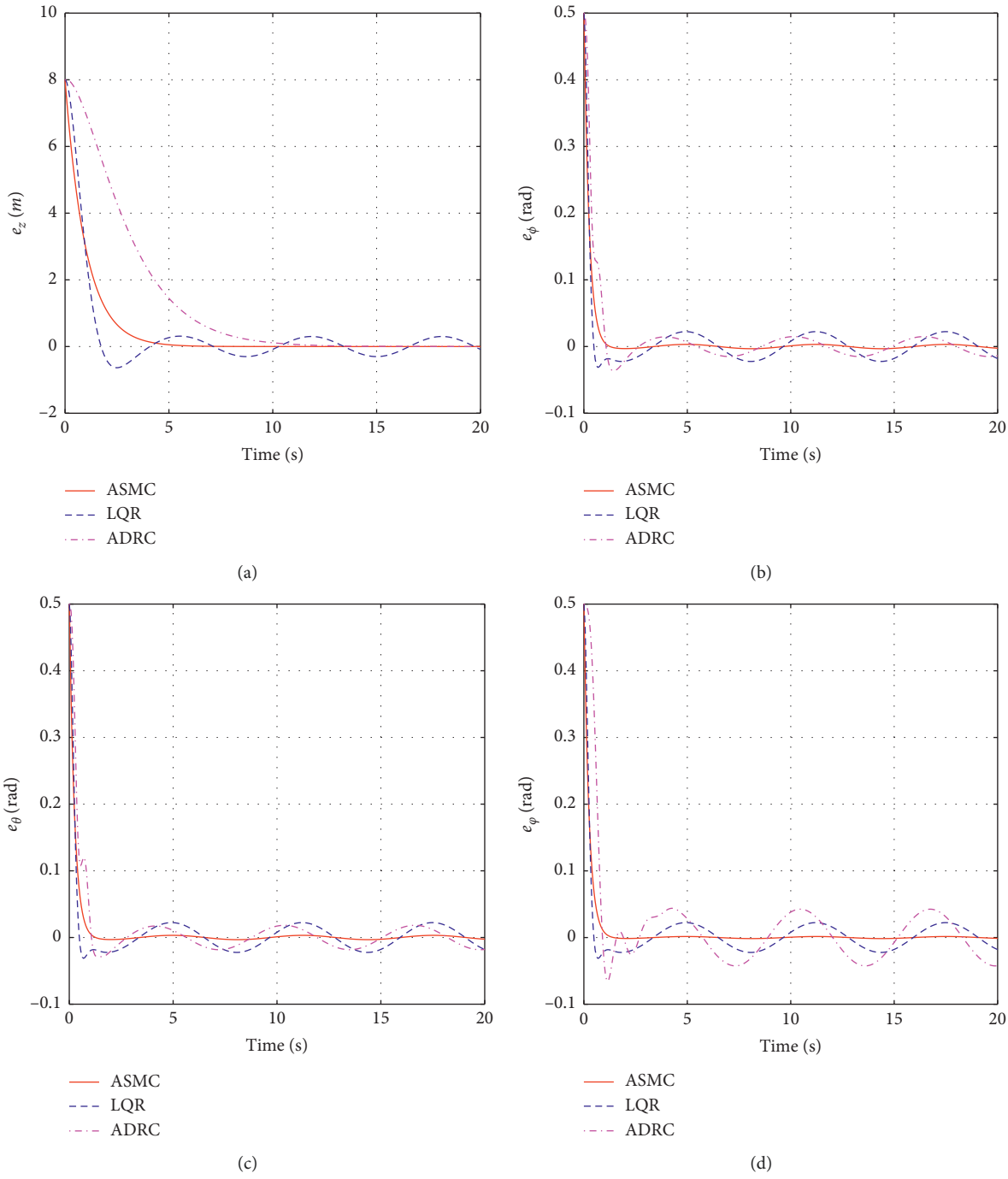

Figure 4: The output tracking error profiles in altitude and attitude control.

Hence, substituting the adaptive laws (35) into (42) and noticing that $|\tilde{d}_\phi| \leq \eta_2$,

$$\begin{aligned}\dot{V}_\phi &= -s_2\eta_2 \mathrm{sgn}(s_2) - k_2 s_2^2 - s_2\tilde{d}_\phi \\ &= -\eta_2|s_2| - k_2 s_2^2 - s_2\tilde{d}_\phi \\ &\leq -k_2 s_2^2 \leq 0,\end{aligned} \tag{43}$$

indicating that $\dot{V}_\phi = 0$ if and only if $s_2 = 0$. Define the set of $\dot{V}_\phi = 0$ as Θ_2, that is, $\Theta_2 = \{(s_2) \mid \dot{V}_\phi = 0\}$. Moreover, Ξ_2 is defined as the largest invariant set in Θ_2. Obviously, the largest invariant set Ξ_2 only includes the point $s_2 = 0$. Therefore, the closed-loop system is asymptotically stabilized, i.e., $s_2 \longrightarrow 0$ when $t \longrightarrow \infty$ according to LaSalle's invariance principle [42]. Observing the detailed expression of the sliding surface (33), the asymptotical convergence of s_2 directly gives that of e_ϕ.

Parallel to the way in designing the control and adaptive laws for the altitude and roll channels, the controller design for the pitch and yaw channels can be derived similarly and given in the following:

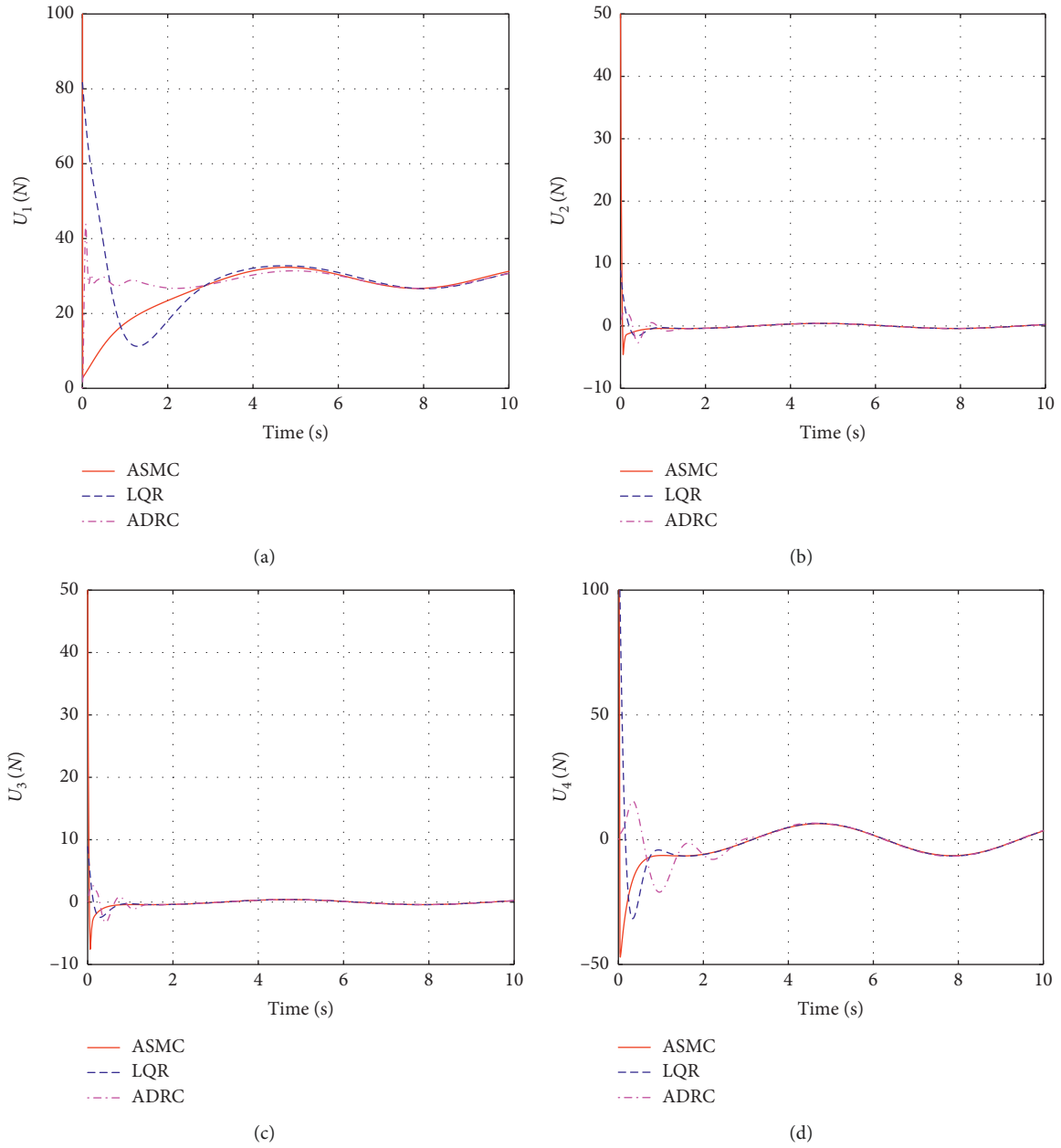

Figure 5: The control input profiles for all the input channels.

$$U_3 = \eta_3 \mathrm{sgn}(s_3) + k_3 s_3 + \hat{\beta}_5 (c_3 \dot{e}_\theta + \ddot{x}_{9d}) - \hat{\beta}_6 x_8 x_{12}, \quad (44)$$

$$\begin{aligned} \dot{\hat{\beta}}_5 &= \gamma_5 s_3 (c_3 \dot{e}_\theta + \ddot{x}_{9d}), \\ \dot{\hat{\beta}}_6 &= -\gamma_6 s_3 x_8 x_{12}, \end{aligned} \quad (45)$$

$$U_4 = \eta_4 \mathrm{sgn}(s_4) + k_4 s_4 + \hat{\beta}_7 \left(c_4 \dot{e}_\varphi + \ddot{x}_{11d}\right) - \hat{\beta}_8 x_8 x_{10}, \quad (46)$$

$$\begin{aligned} \dot{\hat{\beta}}_7 &= \gamma_7 s_4 \left(c_4 \dot{e}_\varphi + \ddot{x}_{11d}\right), \\ \dot{\hat{\beta}}_8 &= -\gamma_8 s_4 x_8 x_{10}, \end{aligned} \quad (47)$$

where c_i, η_i, k_i, $i = 3, 4$, and γ_j, $j = 5, \ldots, 8$ are positive constants, x_{9d} and x_{11d} are the desired pitch and yaw angles, respectively, e_θ and e_φ are the tracking errors of pitch and yaw angles, and s_3 and s_4 are the sliding surfaces, defined as $s_3 = c_3 e_\theta + \dot{e}_\theta$ and $s_3 = c_3 e_\varphi + \dot{e}_\varphi$, respectively. □

Remark 2. It is worth mentioning that since the signum functions are involved in the controllers, chattering phenomenon could be serious when the proposed ASMC laws (22), (34), (44), and (46) are applied in the quadrotor UAV system. To resolve this, saturation functions are used to replace the signum functions in all four channels [40]. The resultant control performance has been verified via simulation and real experiment.

4. Simulation and Experimental Tests

In this section, the effectiveness and robustness of the proposed ASMC scheme will be verified via simulation and real experiment, where the performance of LQR and ADRC are given simultaneously for comparison.

4.1. Simulation. In this part, numerical simulations of the LQR, the ADRC, and the proposed ASMC are implemented via Matlab/Simulink. The model parameters of the quadrotor and the design parameters of the ASMC are listed in Tables 1 and 2, respectively.

The initial altitude and attitude of the quadrotor UAV are set as 0 m and [0, 0, 0] rad. The desired/reference position and attitude are assumed to be $z_d = 8$ m, $\phi_d = \theta_d = \varphi_d = 0.5$ rad, and the external disturbances are $d_x = d_y = d_z = d_\phi = d_\theta = d_\varphi = \sin(t)$.

The time histories of the sliding surfaces are illustrated in Figure 3, revealing the fast convergence of all the sliding surfaces. Figure 4 shows the resulting tracking error profiles for the altitude and attitude control of the quadrotor. It can be seen that, despite the disturbances acting on the system, the errors converge within 5 seconds and become very small after that when applying the proposed ASMC to the quadrotor. The convergence speed and disturbance rejection ability for each channel could be optimized by tuning the magnitudes of c_i, $i = 1, \ldots, 4$ accordingly. Figure 5 shows the time responses of the LQR, the ADRC, and the proposed ASMC (22), (34), (44), and (46) with saturation function. Since the chattering phenomenon is greatly suppressed, the proposed controller can be easily applied in a real quadrotor UAV system.

Comparison with LQR and ADRC has been carried out and the simulation results are presented in Figures 6–9. In Figure 6, we can see that LQR induces a larger overshoot although it has a faster tracking speed for the given reference signal. Meanwhile, the tracking speed of the ASMC is significantly faster than that of the ADRC. In Figures 7–9, the states ϕ, θ, and φ are with smaller vibration when applying the ASMC to the quadrotor system. To sum up, the proposed robust ASMC scheme possesses a better tracking performance for the quadrotor even in the presence of parametric uncertainty and external disturbances.

4.2. Experimental Test. In experiments, the proposed control strategy is applied to a quadrotor UAV platform provided by Beijing Links Tech Co., Ltd., as shown in Figure 10. This platform uses a personal computer (PC), a 51.5 cm × 51.5 cm test bench, an external DC power module, a power adapter, an USB to RS485 converter, a wind speed sensor, and an AR Drone 2.0 quadrotor system with 1 GHz 32 bit ARM Cortex A8 processor, 3-axis gyroscope, 3-axis accelerometer, 3-axis magnetometer, barometer, ultrasonic sensor, 4 brushless motors, 4 motor controllers, and a Wi-Fi wireless module. To ensure the test safety, the quadrotor is fixed on the test platform. Meanwhile, a large and powerful electric fan is used to generate wind disturbance and acts on the quadrotor.

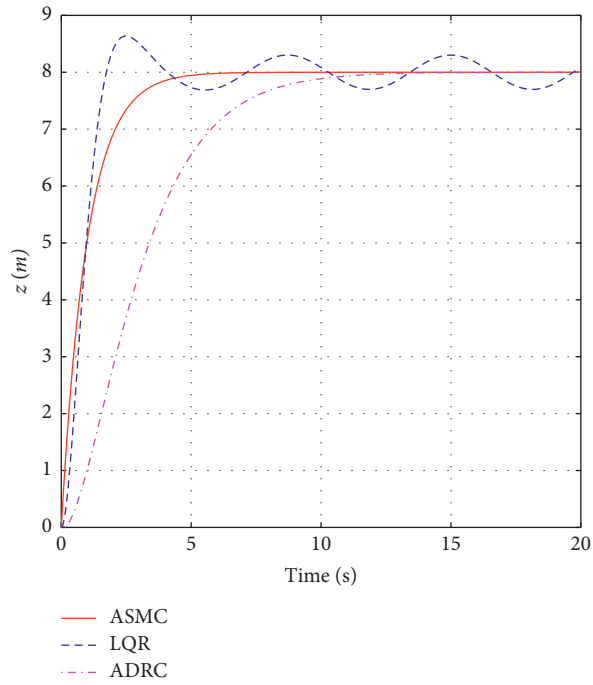

Figure 6: The tracking performance of altitude.

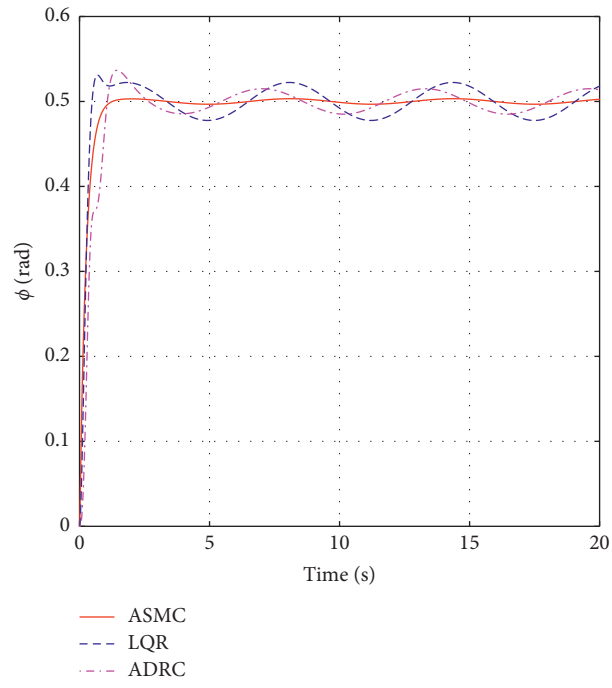

Figure 7: The tracking performance of roll angle.

The controllers are first implemented in Matlab/Simulink. Then, the code generation technique is used to convert the Simulink model into C language code, which is downloaded to the processor via Wi-Fi. It is worth noting

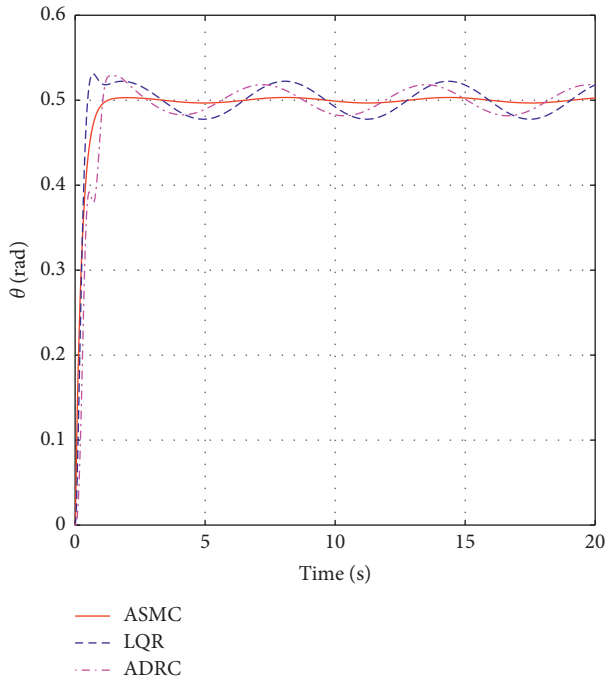

Figure 8: The tracking performance of pitch angle.

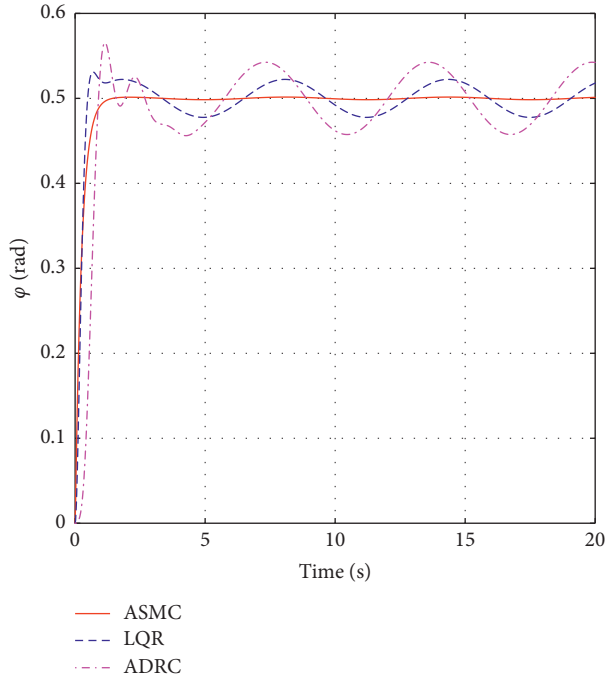

Figure 9: The tracking performance of yaw angle.

that the altitude controller is not verified in experiment, since the altitude of the quadrotor is fixed.

To evaluate the control performance of the three control schemes, including ASMC, LQR, and ADRC, two flight tests with different wind speeds of external disturbance are carried out on the quadrotor platform. Notice that the initial attitudes of the quadrotor could be different in the actual

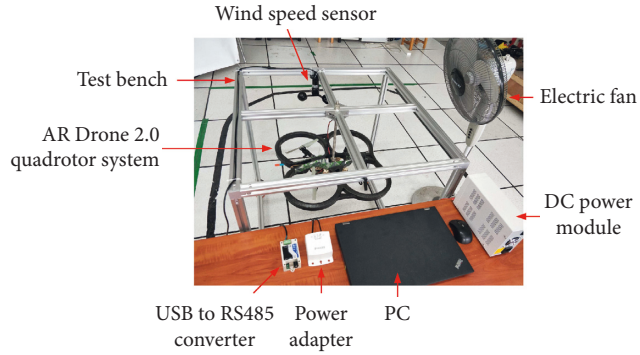

Figure 10: Quadrotor UAV platform.

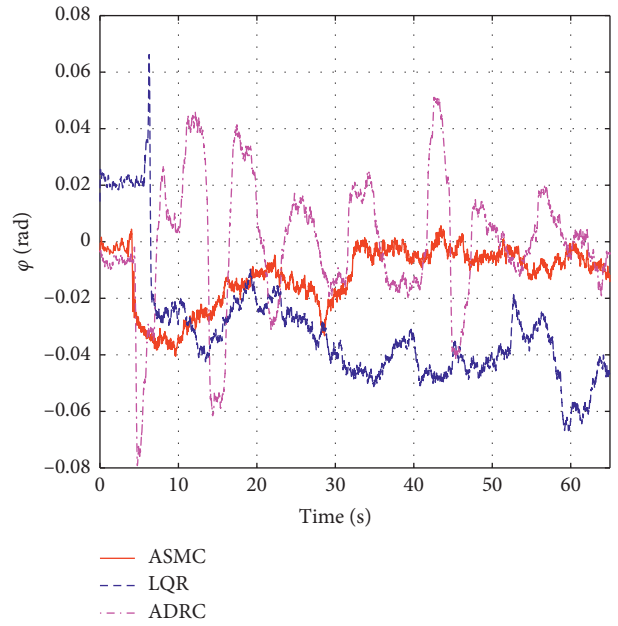

Figure 11: Tracking results of roll angle under the wind speed of 1.6 m/s.

tests, since the attitude of the quadrotor cannot be measured when the quadrotor is in the stationary state.

Case 1. The quadrotor is expected to achieve the reference tracking of roll and pitch angles of 0 rad under the wind speed of 1.6 m/s.

The tracking performance is demonstrated in Figures 11 and 12, where the oscillation generated by the ADRC is more severe than that by the ASMC and the LQR. In Figure 11, the tracking error of the ASMC is obviously smaller than that of the LQR. However, the ASMC and the LQR provide roughly equal control effects in Figure 12. Furthermore, to quantitatively evaluate the attitude angle tracking performance achieved by the proposed ASMC, LQR, and ADRC, two performance indices, i.e., the maximum value of the absolute value of the tracking error (MAE) and the absolute value of the mean tracking error (AME) are used. As listed in Tables 3 and 4, the MAE of the ASMC is smaller than that of the LQR and the ADRC. Meanwhile, the AMEs of the ADRC are

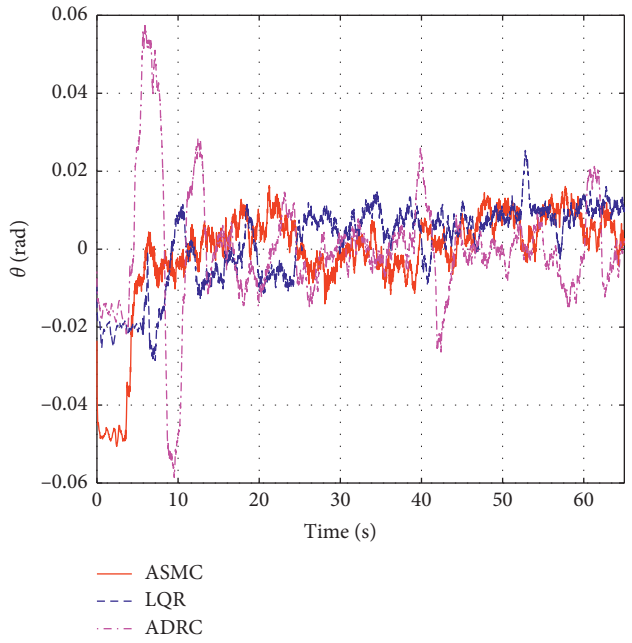

Figure 12: Tracking results of pitch angle under the wind speed of 1.6 m/s.

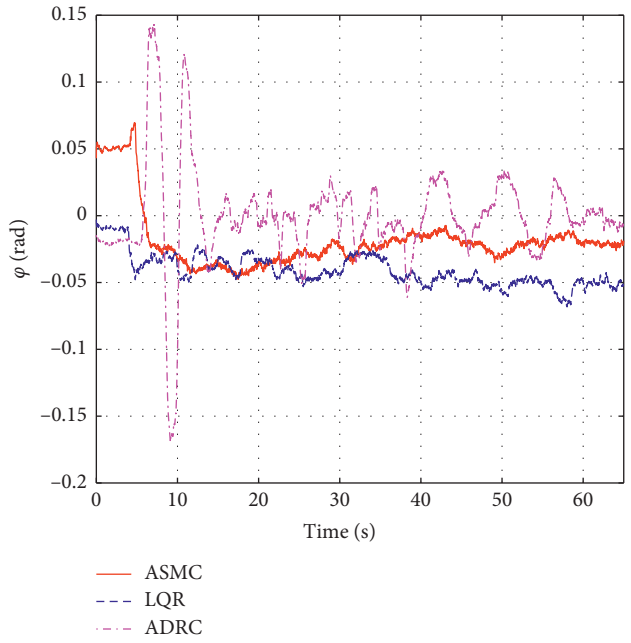

Figure 13: Tracking results of roll angle under the wind speed of 2.8 m/s.

Table 3: Comparison of the roll tracking performance under the wind speed of 1.6 m/s.

Performance index	ASMC	LQR	ADRC
MAE (rad)	0.0359	0.0668	0.0615
AME (rad)	0.0105	0.0375	0.0015

Table 4: Comparison of the pitch tracking performance under the wind speed of 1.6 m/s.

Performance index	ASMC	LQR	ADRC
MAE (rad)	0.0163	0.0253	0.0484
AME (rad)	0.0029	0.0047	4.4182×10^{-4}

clearly the smallest in roll and pitch channels, since the tracking results of roll and pitch have an almost equal amplitude fluctuation above and below zero. In addition, the tracking accuracy obtained from the ASMC is superior to that of LQR in terms of AME.

Case 2. The quadrotor is expected to achieve the reference tracking of roll and pitch angles of 0 rad under the wind speed of 2.8 m/s.

Figures 13 and 14 present the evolution of the attitude of the quadrotor in time. As can be seen from Figure 13, the tracking result of the ADRC has the largest oscillation. The tracking error of the ASMC is significantly smaller than that of the LQR when the time exceeds 30 s. Furthermore, it can be observed from Figure 14 that the ADRC produces the largest overshoot at the beginning of the flight test and that the ASMC has the smallest steady-state error. As a matter of fact, as shown in Tables 5 and 6, ASMC achieves the best tracking performance in roll and pitch channels in terms of the MAE.

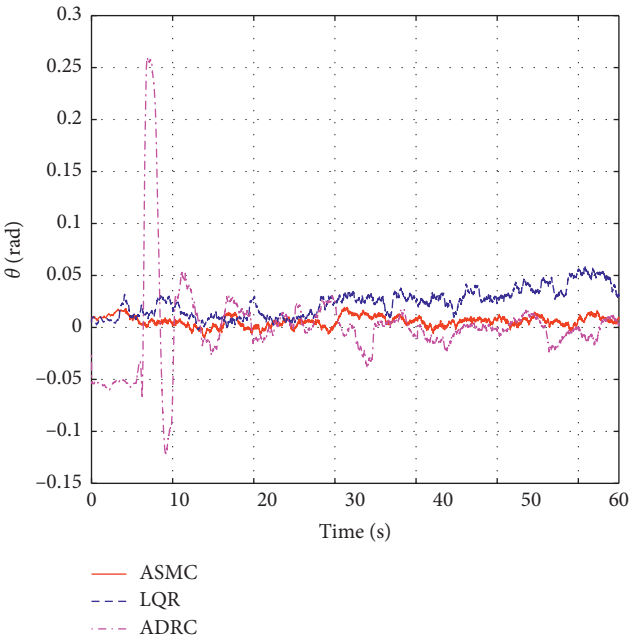

Figure 14: Tracking results of pitch angle under the wind speed of 2.8 m/s.

Table 5: Comparison of the roll tracking performance under the wind speed of 2.8 m/s.

Performance index	ASMC	LQR	ADRC
MAE (rad)	0.0477	0.0682	0.1206
AME (rad)	0.0256	0.0441	9.555×10^{-4}

Table 6: Comparison of the pitch tracking performance under the wind speed of 2.8 m/s.

Performance index	ASMC	LQR	ADRC
MAE (rad)	0.0194	0.0594	0.0642
AME (rad)	0.0054	0.0255	0.0015

Table 7: Controller parameters in the ADRC.

Symbol	Value	Symbol	Value	Symbol	Value	Symbol	Value
r_1	10	r_2	4	r_3	4	r_4	6
h_1	1.6	h_2	0.1	h_3	0.1	h_4	0.3
β_{011}	10	β_{012}	100	β_{013}	100	β_{014}	1
β_{021}	5000	β_{022}	300	β_{023}	300	β_{024}	300
β_{031}	50000	β_{032}	2000	β_{033}	2000	β_{034}	3000
$\underline{b}_{01}$	1	$\underline{b}_{02}$	1	$\underline{b}_{03}$	1	$\underline{b}_{04}$	1
$\underline{\beta}_{11}$	100	$\underline{\beta}_{12}$	20	$\underline{\beta}_{13}$	14	$\underline{\beta}_{14}$	10
$\underline{\beta}_{21}$	100	$\underline{\beta}_{22}$	14	$\underline{\beta}_{23}$	14	$\underline{\beta}_{24}$	14

From the above experimental results and quantitative analysis, it can be concluded that the proposed ASMC control scheme is capable of providing remarkable control performance under the simultaneous effect of parametric uncertainties and external disturbance.

5. Conclusion

A robust ASMC scheme is developed for a quadrotor UAV, which guarantees the asymptotic convergence of the tracking error in altitude and attitude. Adaptive laws are designed for estimation of unknown parameters involved in SMC. A rigorous proof of stability of the proposed control algorithm is accomplished through Lyapunov analysis. Numerical simulation and real experiment have been carried out to verify the effectiveness of the proposed controller. It reveals that the ASMC has a better tracking performance than the LQR or the ADRC in terms of the MAE. Future research will investigate the formation control of the quadrotor UAVs using a multiagent system approach [43–45].

Appendix

Altitude and attitude controllers of the quadrotor based on LQR are given by

$$U_1 = \frac{m}{\cos\phi\cos\theta}\left(g - A_1 x_z + B_1 z_d\right), \tag{A.1}$$

where z_d is the desired altitude and $g = 9.8$, $A_1 = [3.1623, 2.5097]$, $B_1 = 3.1623$, and $x_z = [z, \dot{z}]^T$.

$$\begin{aligned} U_2 &= \frac{J_x}{L}\left(-\frac{J_y - J_z}{J_x}\dot{\theta}\dot{\varphi} - A_2 x_\phi + B_2\phi_d\right),\\ U_3 &= \frac{J_y}{L}\left(-\frac{J_z - J_x}{J_y}\dot{\phi}\dot{\varphi} - A_2 x_\theta + B_2\theta_d\right),\\ U_4 &= \frac{J_z}{f}\left(-\frac{J_x - J_y}{J_z}\dot{\phi}\dot{\theta} - A_2 x_\varphi + B_2\varphi_d\right), \end{aligned} \tag{A.2}$$

where ϕ_d, θ_d, and φ_d are the desired roll, pitch, and yaw angles, respectively, and $A_2 = [44.7214, 9.4574]$, $B_2 = 44.7214$, $x_\phi = [\phi, \dot{\phi}]^T$, $x_\theta = [\theta, \dot{\theta}]^T$, and $x_\varphi = [\varphi, \dot{\varphi}]^T$.

The ADRC scheme can be expressed by

$$U_i = \overline{\beta}_{1i}\left(v_{1i} - z_{1i}\right) + \overline{\beta}_{2i}\left(v_{2i} - z_{2i}\right) - \frac{1}{b_{0i}}z_{3i}, \tag{A.3}$$

$$\begin{aligned} \dot{z}_{1i} &= z_{2i} - \beta_{01i}\left(z_{1i} - y_{0i}\right),\\ \dot{z}_{2i} &= z_{3i} - \beta_{02i}\left(z_{1i} - y_{0i}\right) + b_{0i}U_i,\\ \dot{z}_{3i} &= -\beta_{03i}\left(z_{1i} - y_{0i}\right), \end{aligned} \tag{A.4}$$

$$\begin{aligned} \dot{v}_{1i} &= v_{2i},\\ \dot{v}_{2i} &= \mathrm{fhan}\left(v_{1i} - v_{0i}, v_{2i}, r_i, h_i\right), \end{aligned} \tag{A.5}$$

$$\begin{aligned} d_i &= r_i h_i^2,\\ a_{0i} &= h_i v_{2i},\\ y_i &= \left(v_{1i} - v_{0i}\right) + a_{0i},\\ a_{1i} &= \sqrt{d_i\left(d_i + 8\left|y_i\right|\right)},\\ a_{2i} &= a_{0i} + \frac{\mathrm{sgn}\left(y_i\right)\left(a_{1i} - d_i\right)}{2},\\ a_i &= \left(a_{0i} + y_i\right)\mathrm{fsg}\left(y_i, d_i\right) + a_{2i}\left(1 - fsg\left(y_i, d_i\right)\right),\\ \mathrm{fhan} &= -r_i\frac{a_i}{d_i}\mathrm{fsg}\left(a_i, d_i\right) - r_i\mathrm{sgn}\left(a_i\right)\left(1 - fsg\left(a_i, d_i\right)\right), \end{aligned} \tag{A.6}$$

where $i = 1, \ldots, 4$, v_{0i}, and y_{0i} are the reference signal and output of the controlled plant of the corresponding channel, respectively, and $\mathrm{fsg}(n_1, n_2)$ is described as

$$\mathrm{fsg}\left(n_1, n_2\right) = \frac{\mathrm{sgn}\left(n_1 + n_2\right) - \mathrm{sgn}\left(n_1 - n_2\right)}{2}. \tag{A.7}$$

The design parameters of altitude and attitude controller based on ADRC are listed in Table 7.

Data Availability

All data in the manuscript are available.

Conflicts of Interest

The authors declare that they have no conflicts of interest.

Acknowledgments

The work was supported by the Sichuan Science and Technology Program under Grant nos. 2019YFG0345 and 2019YJ0210, the National Natural Science Foundation of China under Grant nos. 61773323, 61433011, 61603316, and 61733015, and the Fundamental Research Funds for the Central Universities under Grant 2682018CX15.

References

[1] M. S. Kovacevic, K. Gavin, I. S. Oslakovic, and M. Bacic, "A new methodology for assessment of railway infrastructure condition," *Transportation Research Procedia*, vol. 14, no. 14, pp. 1930–1939, 2016.

[2] S. Bertrand, N. Raballand, F. Viguier, and F. Muller, "Ground risk assessment for long-range inspection missions of railways by UAVs," in *Proceedings of the International Conference on Unmanned Aircraft Systems*, pp. 1343–1351, Miami, FL, USA, June 2017.

[3] H. Zhou, H. Kong, L. Wei, D. Creighton, and S. Nahavandi, "Efficient road detection and tracking for unmanned aerial vehicle," *IEEE Transactions on Intelligent Transportation Systems*, vol. 16, no. 1, pp. 297–309, 2015.

[4] J. P. Dash, M. S. Watt, G. D. Pearse, M. Heaphy, and H. S. Dungey, "Assessing very high resolution UAV imagery for monitoring forest health during a simulated disease outbreak," *ISPRS Journal of Photogrammetry and Remote Sensing*, vol. 131, pp. 1–14, 2017.

[5] R. Bhola, N. H. Krishna, K. N. Ramesh, J. Senthilnath, and G. Anand, "Detection of the power lines in UAV remote sensed images using spectral-spatial methods," *Journal of Environmental Management*, vol. 206, pp. 1233–1242, 2018.

[6] B. D. Song, K. Park, and J. Kim, "Persistent UAV delivery logistics: MILP formulation and efficient heuristic," *Computers & Industrial Engineering*, vol. 120, pp. 418–428, 2018.

[7] S. A. Raza, M. Sutherland, J. Etele, and G. Fusina, "Experimental validation of quadrotor simulation tool for flight within building wakes," *Aerospace Science and Technology*, vol. 67, pp. 169–180, 2017.

[8] A. Oosedo, S. Abiko, A. Konno, and M. Uchiyama, "Optimal transition from hovering to level-flight of a quadrotor tail-sitter UAV," *Autonomous Robots*, vol. 41, no. 5, pp. 1143–1159, 2017.

[9] C. Fu, A. Sarabakha, E. Kayacan, C. Wagner, R. John, and J. M. Garibaldi, "Input uncertainty sensitivity enhanced nonsingleton fuzzy logic controllers for long-term navigation of quadrotor UAVs," *IEEE/ASME Transactions on Mechatronics*, vol. 23, no. 2, pp. 725–734, 2018.

[10] N. S. Özbek, M. Önkol, and M. Ö. Efe, "Feedback control strategies for quadrotor-type aerial robots: a survey," *Transactions of the Institute of Measurement and Control*, vol. 38, no. 5, pp. 529–554, 2016.

[11] D. Lee, H. Jin Kim, and S. Sastry, "Feedback linearization vs. adaptive sliding mode control for a quadrotor helicopter," *International Journal of Control, Automation and Systems*, vol. 7, no. 3, pp. 419–428, 2009.

[12] Y. Zhang, Z. Chen, X. Zhang, Q. Sun, and M. Sun, "A novel control scheme for quadrotor UAV based upon active disturbance rejection control," *Aerospace Science and Technology*, vol. 79, pp. 601–609, 2018.

[13] K. Chang, Y. Xia, K. Huang, and D. Ma, "Obstacle avoidance and active disturbance rejection control for a quadrotor," *Neurocomputing*, vol. 190, pp. 60–69, 2016.

[14] K. Alexis, G. Nikolakopoulos, and A. Tzes, "Switching model predictive attitude control for a quadrotor helicopter subject to atmospheric disturbances," *Control Engineering Practice*, vol. 19, no. 10, pp. 1195–1207, 2011.

[15] A. T. Hafez, S. N. Givigi, and S. Yousefi, "Unmanned aerial vehicles formation using learning based model predictive control: UAVs formation using learning based model predictive control," *Asian Journal of Control*, vol. 20, no. 3, pp. 1014–1026, 2018.

[16] Y. Bouzid, H. Siguerdidjane, and Y. Bestaoui, "Nonlinear internal model control applied to vtol multi-rotors UAV," *Mechatronics*, vol. 47, pp. 49–66, 2017.

[17] B. Tian, L. Liu, H. Lu, Z. Zuo, Q. Zong, and Y. Zhang, "Multivariable finite time attitude control for quadrotor UAV: theory and experimentation," *IEEE Transactions on Industrial Electronics*, vol. 65, no. 3, pp. 2567–2577, 2018.

[18] R. Wang and J. Liu, "Trajectory tracking control of a 6-dof quadrotor UAV with input saturation via backstepping," *Journal of the Franklin Institute*, vol. 355, no. 7, pp. 3288–3309, 2018.

[19] C. Li, Y. Zhang, and P. Li, "Full control of a quadrotor using parameter-scheduled backstepping method: implementation and experimental tests," *Nonlinear Dynamics*, vol. 89, no. 1, pp. 1–20, 2017.

[20] L. Cao, X. Hu, S. Zhang, and Y. Liu, "Robust flight control design using sensor-based backstepping control for unmanned aerial vehicles," *Journal of Aerospace Engineering*, vol. 30, no. 6, Article ID 04017068, 2017.

[21] S. Mobayen, "A novel global sliding mode control based on exponential reaching law for a class of underactuated systems with external disturbances," *Journal of Computational and Nonlinear Dynamics*, vol. 11, no. 2, p. 9, 2016.

[22] R. Xu and Ü. Özgüner, "Sliding mode control of a class of underactuated systems," *Automatica*, vol. 44, no. 1, pp. 233–241, 2008.

[23] M. J. Reinoso, L. I. Minchala, P. Ortiz, D. F. Astudillo, and D. Verdugo, "Trajectory tracking of a quadrotor using sliding mode control," *IEEE Latin America Transactions*, vol. 14, no. 5, pp. 2157–2166, 2016.

[24] F. Muñoz, I. González-Hernández, S. Salazar, E. S. Espinoza, and R. Lozano, "Second order sliding mode controllers for altitude control of a quadrotor uas: real-time implementation in outdoor environments," *Neurocomputing*, vol. 233, pp. 61–71, 2017.

[25] W. Zhou, P. Zhu, C. Wang, and M. Chu, "Position and attitude tracking control for a quadrotor UAV based on terminal sliding mode control," in *Proceedings of the 34th Chinese Control Conference*, pp. 3398–3404, Hangzhou, China, July 2015.

[26] J. J. Xiong and G. B. Zhang, "Global fast dynamic terminal sliding mode control for a quadrotor UAV," *ISA Transactions*, vol. 66, pp. 233–240, 2016.

[27] H. Ríos, J. González-Sierra, and A. Dzul, "Robust tracking output-control for a quad-rotor: a continuous sliding-mode approach," *Journal of the Franklin Institute*, vol. 354, no. 15, pp. 6672–6691, 2017.

[28] A. Basci, K. Can, K. Orman, and A. Derdiyok, "Trajectory tracking control of a four rotor unmanned aerial vehicle based on continuous sliding mode controller," *Elektronika ir Elektrotechnika*, vol. 23, no. 3, pp. 12–19, 2017.

[29] C. Izaguirre-Espinosa, V. Parra-Vega, P. Castillo, A. J. Muñoz-Vázquez, and A. Sánchez-Orta, "Attitude control of quadrotors based on fractional sliding modes: theory and experiments," *IET Control Theory & Applications*, vol. 10, no. 7, pp. 825–832, 2016.

[30] C. Izaguirre-Espinosa, A.-J. Muñoz-Vázquez, A. Sanchez-Orta, V. Parra-Vega, and P. Castillo, "Contact force tracking of quadrotors based on robust attitude control," *Control Engineering Practice*, vol. 78, pp. 89–96, 2018.

[31] Y.-R. Tang, X. Xiao, and Y. Li, "Nonlinear dynamic modeling and hybrid control design with dynamic compensator for a small-scale UAV quadrotor," *Measurement*, vol. 109, pp. 51–64, 2017.

[32] F. Chen, R. Jiang, K. Zhang, B. Jiang, and G. Tao, "Robust backstepping sliding-mode control and observer-based fault estimation for a quadrotor UAV," *IEEE Transactions on Industrial Electronics*, vol. 63, no. 8, pp. 5044–5056, 2016.

[33] G. V. Raffo, M. G. Ortega, and F. R. Rubio, "An integral predictive/nonlinear h_∞ control structure for a quadrotor helicopter," *Automatica*, vol. 46, no. 1, pp. 29–39, 2010.

[34] Z. Xu, X. Nian, H. Wang, and Y. Chen, "Robust guaranteed cost tracking control of quadrotor UAV with uncertainties," *ISA Transactions*, vol. 69, pp. 157–165, 2017.

[35] H. Liu, J. Xi, and Y. Zhong, "Robust attitude stabilization for nonlinear quadrotor systems with uncertainties and delays," *IEEE Transactions on Industrial Electronics*, vol. 64, no. 7, pp. 5585–5594, 2017.

[36] N. Fethalla, M. Saad, and H. Michalska, "Robust observer-based dynamic sliding mode conroller for a quadrotor UAV," *IEEE Access*, vol. 6, pp. 45846–45859, 2018.

[37] S. Li, Y. Wang, J. Tan, and Y. Zheng, "Adaptive rbfnns/integral sliding mode control for a quadrotor aircraft," *Neurocomputing*, vol. 216, pp. 126–134, 2016.

[38] O. Mofid and S. Mobayen, "Adaptive sliding mode control for finite-time stability of quad-rotor UAVs with parametric uncertainties," *ISA Transactions*, vol. 72, pp. 1–14, 2018.

[39] G. Perozzi, D. Efimov, J. Biannic, and L. Planckaert, "Trajectory tracking for a quadrotor under wind perturbations: sliding mode control with state-dependent gains," *Journal of the Franklin Institute*, vol. 355, no. 12, pp. 4809–4838, 2018.

[40] B. Abci, G. Zheng, D. Efimov, and M. E. B. E. Najjar, "Robust altitude and attitude sliding mode controllers for quadrotors," in *Proceedings of World Congress of the International Federation of Automatic Control*, pp. 2720–2725, Toulouse, France, July 2017.

[41] A. Poutney, C. Kennedy, G. Clayton, and H. Ashrafiuon, "Robust tracking control of quadrotors based on differential flatness: simulations and experiments," *IEEE/ASME Transactions on Mechatronics*, vol. 23, no. 3, pp. 1126–1137, 2018.

[42] N. Sun, T. Yang, H. Chen, Y. Fang, and Y. Qian, "Adaptive anti-swing and positioning control for 4-dof rotary cranes subject to uncertain/unknown parameters with hardware experiments," *IEEE Transactions on Systems, Man, and Cybernetics: Systems*, vol. 49, no. 7, pp. 1309–1321, 2019.

[43] J. Xi, M. He, H. Liu, and J. Zheng, "Admissible output consensualization control for singular multi-agent systems with time delays," *Journal of the Franklin Institute*, vol. 353, no. 16, pp. 4074–4090, 2016.

[44] L. Wang, J. Xi, M. He, and G. Liu, "Robust time-varying formation design for multi-agent systems with disturbances: extended-state-observer method," 2019, https://arxiv.org/abs/1909.08974.

[45] J. Xi, C. Wang, X. Yang, and B. Yang, "Limited-budget output consensus for descriptor multiagent systems with energy constraints," 2019, https://arxiv.org/abs/1909.08345.